Theory of a Josephson junction parallel array detector sensitive to very weak signals

D. Chevriaux,[1] R. Khomeriki,[1,2,3] and J. Leon[1]
[1]*Laboratoire de Physique Théorique et Astroparticules CNRS-UMR5207, Université Montpellier 2, 34095 Montpellier, France*
[2]*Dipartimento di Energetica S. Stecco, Universita di Firenze, 50139 Firenze, Italy*
[3]*Department of Physics, Tbilisi State University, 0128 Tbilisi, Georgia*
(Received 12 February 2006; revised manuscript received 15 May 2006; published 14 June 2006)

An array of coupled short junctions (Josephson junction parallel array) is shown to be able to response to ultra-weak signals when it is worked at the onset of nonlinear supratransmission in the hysteresis loop of bistability. The theory is based on the fundamental solutions of the continuous limit (the sine-Gordon equation on the finite interval submitted to Neuman boundary conditions) that result from synchronization and adaptation to the external driving. This provides the solution to a problem that dates back to 1986 [O. H. Olsen and M. R. Samulsen, Phys. Rev. B **34**, 3510 (1986)], namely the complete analytical understanding of the bistability in a long Josephson junction or in an array of short junctions. The property allows to conceive ultrasensitive detectors or else, by convenient modulation of the seed, efficient digital amplifiers. Numerical simulations reveal that such a bistable behavior occurs also in two-dimensional lattices where no theory is available yet.

DOI: 10.1103/PhysRevB.73.214516 PACS number(s): 74.81.Fa, 85.25.Cp, 42.65.Wi, 05.45.−a

I. INTRODUCTION

Nonlinearly induced bistability has become a major issue in recent years to conceive ultrasensitive detectors, switches, amplifiers, or permanent memories. In particular, nonlinear bistability in a long Josephson junction submitted to microwave irradiation has been unveiled two decades ago by means of numerical simulations of the driven and damped sine-Gordon equation.[1] It has been further extended in Ref. 2 to arrays of short superconducting tunnel junctions coupled through superconducting wires, the so called *Josephson junction (JJ) parallel array*.[3] An interpretation of nonlinear bistability in that context has been built by perturbative analysis in Ref. 4, but a comprehensive analytical description was still missing. The story of *nonlinear bistability* actually began in periodic dielectric (Bragg) media when they are worked in the Kerr regime within the forbidden bandgap.[5]

This theoretical study intends first to provide the complete analytical background for the bistability property of a JJ parallel array, as well as of a long Josephson junction (for a review, see Refs. 6 and 7). It allows us, in particular, to determine the *supratransmission threshold* where the system starts to absorb energy from the external driving, undergoing a bifurcation from a state of low transmissivity to a state of high transmissivity.

As an important application of this result, we then demonstrate that one may use a JJ parallel array at the *onset of supratransmission* to conceive detectors of ultraweak signals. A scheme of the device is represented in Fig. 1, where $I_s(t)$ is the radio-frequency seed with a frequency Ω in the forbidden band, $S(t)$ is the signal to be detected, and I_{out} is the measured output rf current (one actually measures its root of the mean square value).

Highly sensitive detectors have been recently conceived with a short Josephson junction. In that case it is not nonlinear bistability but rather *nonlinear bifurcation* (separatirx crossing) that is used to realize an amplificator that *"remains efficient at the quantum limit."*[8,9] The single junction is driven by an external rf seed tuned to the resonant frequency at an amplitude such that the oscillations reach the separatrix. Any superimposed rf signal at the same (resonant) frequency will then make the junction to jump to the rotating state.

Our device, thought of as a detector, will then be shown to possess a set of intrinsic qualities. First, the detection of *any signal* (no condition on the frequency), second a working regime at *tunable seed intensity* (tuned by choosing the frequency value), third an *adjustable sensitivity* (adjusted by choosing the seed intensity value, respectively, with the supratransmission threshold). These properties are demonstrated by deriving analytical expressions of the solutions and by checking the predicted behaviors on numerical simulations. We display, for instance, later in Fig. 5, a typical numerical simulation with four junctions that shows the output current intensity I_{out} when the first junction is subjected to a driving seed $I_s(t)$ and a low amplitude signal kick $S(t)$, as described in the caption.

The bistability property of the device is then shown also to be a means to realize a *digital amplifier* by a convenient

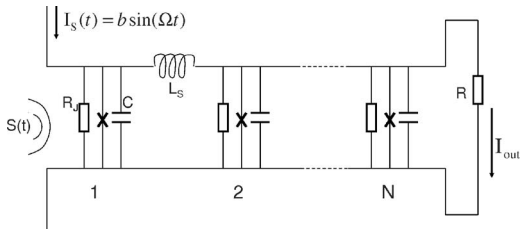

FIG. 1. Schematic representation of the JJ parallel array built with N junctions. $I_S(t)$ is the injected seed current with frequency Ω in the forbidden bandgap and intensity b. $S(t)$ represents the signal to be detected by reading the output current intensity I_{out}. When b is tuned close to the supratransmission threshold, the device works as an ultrasensitive detector. By a convenient slow modulation of b, it then works as a digital amplifier.

modulation of the seed. In that case the seed and the signal (to be amplified) possess the same frequecy, and the role of the seed modulation is to allow the system to jump to an excited state (under action of the signal) and to settle back (after signal extinction). An instance of such a working regime is displayed later in Fig. 6.

In the continuous limit, used to derive explicit solutions, the model describes a long Josephson junction for which our analysis thus allows us to conceive also ultrasensitive detectors or digital amplifiers. Last, in the case of a two-dimensional (square) lattice we have obtained by numerical simulations that the bistability still works, though no theoretical prediction has been made so far. This result opens interesting theoretical problems for the sine-Gordon model in 2+1 dimensions, together with appealing experimental questions.

II. THE JOSEPHSON JUNCTION PARALLEL ARRAY

Let us consider a one-dimensional array of N short Josephson junctions coupled through superconducting wires, as represented by Fig. 1. It obeys the following model:[3]

$$\ddot{u}_1 + \gamma\dot{u}_1 - \lambda_J^2[u_2 - u_1] + \sin u_1 = f(t), \tag{1}$$

$$\ddot{u}_n + \gamma\dot{u}_n - \lambda_J^2[u_{n+1} + u_{n-1} - 2u_n] + \sin u_n = 0, \tag{2}$$

$$\ddot{u}_N + \gamma\dot{u}_N - \lambda_J^2[u_{N-1} - u_N] + \sin u_N = -I_{\text{out}}, \tag{3}$$

for $n=2,\ldots,N-1$ and where both $f(t)$ and I_{out} are normalized to the Josephson critical current I_c in the single junction. The time is normalized to the inverse plasma frequency $\omega_p = 1/\sqrt{L_J C}$, C stands for the junction capacitance, and $L_J = \hbar/(2eI_c)$ is the Josephson inductance. The parameter λ_J is defined by $\lambda_J^2 = L_J/L_S$, where L_S is the inductance representing by the superconducting wires connecting the junctions. $\gamma = \sqrt{\hbar/(2eI_cR^2C)}$ is a damping parameter, and R the junction resistance. In typical experiments on the Josephson junction parallel array, as in, Ref. 3 the parameters have the values: $R \approx 100\ \Omega$, $C \approx 300$ fF, $I_c \approx 10\ \mu$A, $L_S \approx$ pH and thus $\gamma \approx 0.1$ and $\lambda_J \approx 3$. However, by changing the critcal current density and the temperature, one can easily control the two parameters of the mode γ and λ_J. For our numerical simulations we choose $\lambda_J = 2$ and $\gamma = 0.02$.

By using now the Ohmic law $I_{\text{out}} = V_{\text{out}}/R = \dot{u}_N/R$, where R is the output reading resistance, (3) can be rewritten as

$$\ddot{u}_N + (\gamma + 1/R)\dot{u}_N - \lambda_J^2(u_{N-1} - u_N) + \sin u_N = 0. \tag{4}$$

The driving $f(t)$ is made of a periodic seed $I_s(t)$ with its frequency Ω in the natural band gap ($\Omega < 1$), to which an arbitrary, low amplitude, finite time signal $S(t)$ is superimposed, namely

$$f(t) = I_s(t) + S(t). \tag{5}$$

As the presence of an external signal actually modifies the value of the seed, the above summation of the seed and the signal is not exact. However, as far as the signal is assumed to be very small, it makes inessential changes to the finite seed current. Moreover, it should be mentioned that $S(t)$ expresses the contribution of electric and magnetic fields of the signal, as found in Refs. 10 and 11. In order to avoid the initial shock on a system initially at rest, $I_s(t)$ will be settled after a transient sequence, where it grows from a vanishing amplitude to its actual value.

It is convenient to define two virtual junctions in $n=0$ and $n=N+1$ by setting

$$u_0 - u_1 \equiv f(t), \quad u_{N+1} - u_N \equiv 0, \tag{6}$$

such that the continuous limit (large λ_J and N) becomes the sine-Gordon equation,

$$x \in [0,L]: u_{tt} + \gamma u_t - u_{xx} + \sin u = 0, \tag{7}$$

in the variable $x = n/\lambda_J$. It is associated to the Neuman boundary value problem that automatically follows from (6),

$$u_x(0,t) = -f(t)/\lambda_J, \quad u_x(L,t) = 0, \tag{8}$$

on a vanishing initial state $u(x,0) = u_t(x,0) = 0$.

The measure of I_{out} as indicated in Fig. 1 implies that the value of the damping coefficient γ in (7) should be changed to $\gamma + 1/R$ in $x=L$. Thus, keeping γ constant (as we do hereafter to derive explicit solutions) simply means that our results hold for large values of R. However, the nature of the observed phenomena does not change for smaller R, only the agreement between numerical simulations and theory will be less accurate.

Let us remark that the above continuous version is also a model for a long Josephson junction whose extremity $x=0$ is submitted to external microwave irradiation, $f(t)$ being then related to the external magnetic field intensity.[12]

III. METHOD AND SOLUTIONS

In order to describe the periodic stationary asymptotic regimes, we seek a solution to (7) with $\gamma=0$, submitted to the Neuman boundary condition (8), where $f(t)$ has the periodic structure

$$f(t) = b\sin(\Omega t), \quad \Omega < 1, \tag{9}$$

under the general expression[13]

$$u(x,t) = 4\arctan[X(x)T(t)]. \tag{10}$$

The product XT allowing for an arbitrary normalization, we choose to scale $T(t)$, over a period, to the amplitude value 1, namely

$$\max_t |T(t)| = 1. \tag{11}$$

Then the boundary-value problem is solved by requiring *adaptation* and *synchronization* to the driver, namely,

$$\frac{4X'(0)}{1 + X(0)^2} = \frac{b}{\lambda_J}, \quad T\left(t + \frac{2\pi}{\Omega}\right) = T(t). \tag{12}$$

Note that the adaptation to the driver is nothing but the expression of the boundary value (8) in $x=0$, while the synchronization condition, namely that the solution acquires the

period of the driver, is by no way evident in a nonlinear system. Here it is actually validated by numerical simulations where the damping allows the system to settle down to the predicted stationary regimes.

Finally, the right-hand side Neuman boundary condition $u_x(L,t)=0$ can be written as

$$X'(L)=0, \quad X(L)=A, \tag{13}$$

where the amplitude parameter A is the unknown to be solved for. Actually, our method consists in fixing the unknown A and seeking the corresponding values of the input b. Indeed the exact analytical solution of (7) is uniquely defined from the values L, A, and Ω. The adaptation condition in (12) then provides a closed relation between the driving amplitude b and the output amplitude A (or equivalently $B=4\arctan A$) for each given length L and frequency Ω.

The solutions are now obtained by inserting the expression (10) in the sine-Gordon equation and expressing the above four boundary constraints in (12) and (13). The technical calculation is standard (see, e.g., Ref. 14), and we shall not give details here. The point is that there are three different ranges for the value of A which give rise to three different solutions, and consequently to the bistable nature of the system.

Solution of type I. For $A>A_1=\sqrt{1-\Omega^2}/\Omega$, we obtain the solution

$$u^I(x,t)=4\arctan\{A\,\mathrm{cn}[k_1(x-L),\mu_1]\mathrm{cn}[\omega_1 t,\nu_1]\}, \tag{14}$$

where $\mathrm{cn}(\cdot,m)$ is the cosine-amplitude Jacobi elliptic function of modulus m. The parameters ω_1 and ν_1 are expressed via A and Ω by the solution of the system

$$\omega_1^2=\frac{A^2}{1+A^2}\frac{1}{A^2-\nu_1^2(1+A^2)}, \quad \frac{\pi}{2}\frac{\omega_1}{\Omega}=\mathbb{K}(\nu_1), \tag{15}$$

where $\mathbb{K}$ is the complete elliptic integral of the first kind. The second relation of (15) guarantees that the actual period of (14) obeys the synchronization condition (12). The remaining parameters k_1, and μ_1 are finally defined explicitly from A, Ω, and ν_1 by

$$k_1^2=\frac{1}{1+A^2}\frac{A^4-A^4\nu_1^2+\nu_1^2}{A^2-\nu_1^2(1+A^2)}, \quad \mu_1^2=\frac{A^4(1-\nu_1^2)}{A^4(1-\nu_1^2)+\nu_1^2}. \tag{16}$$

Solution of type II. Another solution holds in the case $A_0<A<A_1$, where A_0 is the solution of

$$\Omega\mathbb{K}(A_0^2)=\frac{\pi}{2(1+A_0^2)}. \tag{17}$$

This solution reads as

$$u^{II}(x,t)=4\arctan\{A\,\mathrm{dn}[k_2(x-L),\mu_2]\mathrm{sn}[\omega_2 t,\nu_2]\}, \tag{18}$$

where similarly ω_2 and ν_2 solve the system

$$\omega_2^2=\frac{A^2}{(1+A^2)(A^2+\nu_2^2)}, \quad \frac{\pi}{2}\frac{\omega_2}{\Omega}=\mathbb{K}(\nu_2), \tag{19}$$

and where k_2 and μ_2 are given by the expressions

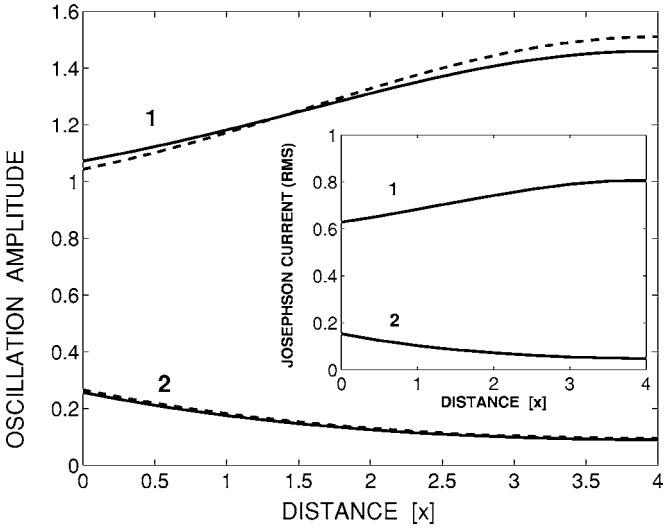

FIG. 2. Analytic solutions (dashed lines) corresponding to the single driving amplitude $b=0.1$ and frequency $\Omega=0.9$, compared to numerical simulations (solid lines) of the continuous model (7) of length $L=4$. The two regimes correspond to the points 1 and 2 of the picture in Fig. 3. The inset shows the corresponding rms values of the Josephson current (23).

$$k_2^2=\frac{A^4}{(1+A^2)(A^2+\nu_2^2)}, \quad \mu_2^2=1-\frac{\nu_2^2}{A^4}. \tag{20}$$

Solution of type III. Finally, for $A<A_0$ we have the solution

$$u^{III}(x,t)=4\arctan\left(\frac{A\,\mathrm{sn}[\omega_2 t,\nu_2]}{\mathrm{dn}[k_3(x-L),\mu_3]}\right), \tag{21}$$

where ω_2 and ν_2 are already expressed by (19) and where the explicit values of the parameters k_3 and μ_3 are

$$k_3^2=\frac{\nu_2^2}{(1+A^2)(A^2+\nu_2^2)}, \quad \mu_3^2=1-\frac{A^4}{\nu_2^2}. \tag{22}$$

For a given driving intensity $b=0.1$ at frequency $\Omega=0.9$, we display in Fig. 2 the comparison between the actual profiles of the amplitudes of the stationary solutions u^{III} and u^{II} (dashed lines) and the results of numerical simulations (full lines) of the sine-Gordon model (7). Moreover, in the inset of the same picture we present the root of mean square values (rms) of the Josephson current,

$$\langle I\rangle(x)=\left(\frac{1}{\mathcal{T}}\int_0^{\mathcal{T}} dt\,\sin^2 u(x,t)\right)^{1/2}, \tag{23}$$

in both regimes ($\mathcal{T}$ is the driving period $2\pi/\Omega$). Note, in particular, the drastic difference between the rms intensity values in the last junction ($x=L$) in the two regimes.[15]

It is quite remarkable that the solution locks precisely to one of the particular solutions (here u^{II} or u^{III}), which thus furnish a complete theoretical ground for the bistability process[16] (note that the damping $\gamma\dot{u}_n$ allows the solution to reach effectively the stationary regimes).

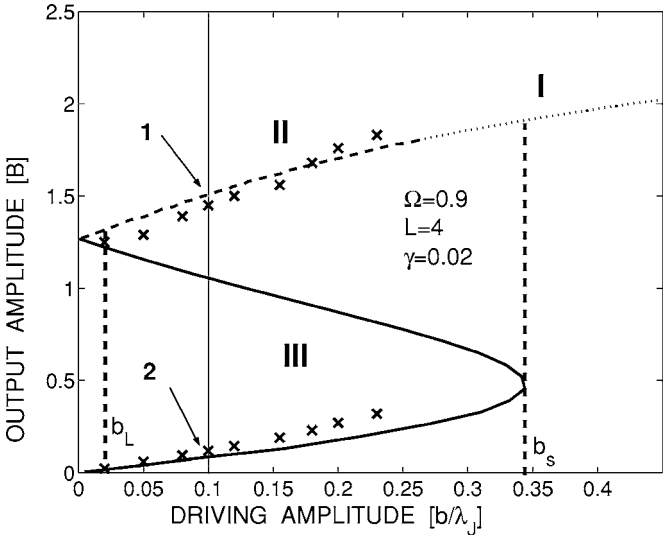

FIG. 3. Dependence of the output amplitude (B) on the driving amplitude (b). The full line stands for (26), the dashed line for (25), and the dotted line for (24). Crosses are the results of numerical simulations of (2) with $N=8$, $\gamma=0.02$, and $\lambda_J=2$. The dashed vertical line b_s indicates the supratransmission threshold (theory). The lower threshold b_L is the phenomenological amplitude value where the solution II settles down to solution III by effect of damping, thus closing the hysteresis loop.

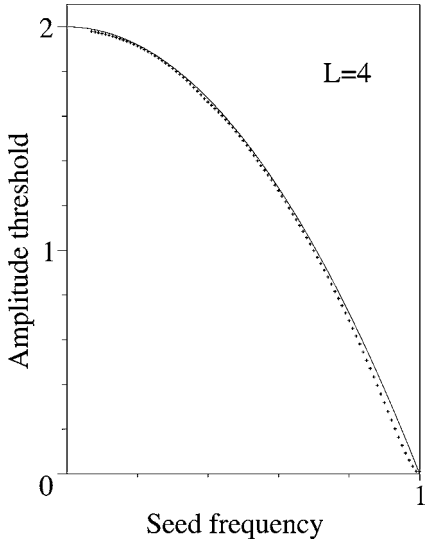

FIG. 4. Dots: plot of the threshold b_s in terms of the driver's frequency Ω, obtained in the continuous case with $L=4$ (corresponding to the discrete case $N=8$ and $\lambda_j=2$). The full line is the approximate expression (27) predicted by the limit $L\to\infty$.

IV. HYSTERESIS LOOP, SUPRATRANSMISSION THRESHOLD

The explicit solutions (14), (18), and (21), provide the driving amplitude b by requiring that the system response adapts according to (12). Then for the boundary condition (8) and driver amplitude definition (9) one has the three functions $b(A)$,

$$A_1 < A, \quad b = 4\lambda_J \frac{\partial}{\partial L} \arctan[A\ \mathrm{cn}(k_1 L, \mu_1)], \tag{24}$$

$$A \in [A_0, A_1], \quad b = 4\lambda_J \frac{\partial}{\partial L} \arctan[A\ \mathrm{dn}(k_2 L, \mu_2)], \tag{25}$$

$$A < A_0, \quad b = 4\lambda_J \frac{\partial}{\partial L} \arctan[A/\mathrm{dn}[k_3 L, \mu_3]], \tag{26}$$

where the parameters k_j and μ_j are given in terms of A in (16), (20), and (22).

By inverting the above expressions for a given input amplitude b, we obtain three solutions for the output amplitude $B=4\arctan A$. Figure 3 displays the plot of $B(b)$ compared to numerical simulations of (2). Though being done for the discrete system ($N=8$, $\lambda_J=2$) the agreement with the continuous theory is striking. In practice, the system first jumps to the state u^I and then, by the effect of damping, settles down to the regime u^{II}. The jump in the hysteresis loop works by exceeding the threshold b_s referred to as *nonlinear supratransmission threshold* defined in the the semi-infinite line case.[17] The threshold b_s is defined here as the value of b, where the derivative of the function $b(B)$ in (26) diverges. It provides a quite involved implicit expression wich is evaluated numerically and displayed in Fig. 4.

It is remarkable that the supratransmission threshold of the infinite line case given in Ref. 18, namely,

$$b_\infty(\Omega) = 2(1-\Omega^2), \tag{27}$$

fits reasonably well the $L=4$ case, the agreement being better for larger L. The knowledge of $b_s(\Omega)$, or its approximate value $b_\infty(\Omega)$, then provides a useful tool to determine either at which frequency one has to work when the seed intensity is constrained, or else what should be the intensity when the frequency is fixed. The sensitivity then depends on how far from the threshold curve of Fig. 4 one is working.

V. ULTRASENSITIVE SIGNAL DETECTOR

In order to show that the JJ parallel array can be used as a detector sensitive to a very weak arbitrary signal, we chose for the definition (5) the following class of external driving:

$$I_s(t) = b\sin(\Omega t), \quad S(t) = \frac{\alpha}{\cosh[\beta(t-t_0)]}. \tag{28}$$

The seed $I_s(t)$ has a frequency in the forbidden bandgap ($\Omega<1$) and an amplitude close to the supratransmission threshold $b_s(\Omega)$. The signal $S(t)$ is chosen here as a localized kick and we solve numerically the system (1)–(3).

A typical result is displayed in Fig. 5, where the small amplitude signal has allowed the system to jump to the excited state with correspondingly a high output current. The corresponding rms values, computed from expression (23), jump from 0.0041 to 0.01. The seed to signal amplitude ratio is here about 2×10^{-2}, which can even be improved by working closer to the threshold, and that justifies the denomination of the *ultrasensitive detector*.

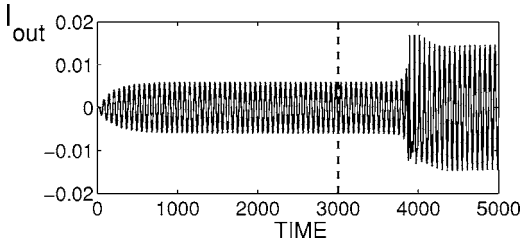

FIG. 5. Time dynamics of of the measurable output current I_{out} obtained via numerical simulations of (1)–(3) for $N=4$, $\lambda_J=2$, $\gamma=0.01$, and $R=100$. The excitation (9) is constituted of an amplitude seed $b=0.363\,91$, a frequency $\Omega=0.9$, and a signal $S(t)=0.01/\cosh[0.1(t-3000)]$. The vertical dashed line shows the time of the signal kick.

VI. DIGITAL AMPLIFIER

Another application is the digital amplifier, where the seed signal amplitude is modulated such as to vary between two values, say A_2 and A_1, both slightly below the thresholds b_s (supratransmission) and b_L (extinction), respectively, as obtained by numerical simulations reported in Fig. 3. Precisely, we set

$$I_s(t) = \frac{1}{2}\cos(\Omega t)[(A_2 - A_1)\sin(\lambda t) + A_2 + A_1]. \quad (29)$$

The signal $S(t)$ is made of a sequence of low amplitude finite time excitations at the frequency Ω of the seed. The duration of every individual signal should exceed the period of the modulation, such as to let the system bifurcate to the excited state. Moreover, the time separation of two successive signals should also exceed the modulation period to let the system settle back to the nonexcited regime. To give an example, we may use the following analytic model of a sequence of two signals (that can be extended to any number),

$$S(t) = \cos(\Omega t)[\alpha_1 F(t_1,t_2) + \alpha_2 F(t_3,t_4)], \quad (30)$$

where $F(t_i,t_j)$ denotes the normalized step of support $[t_i,t_j]$ namely (θ is the Heaviside distribution)

$$F(t_i,t_j) = \theta(t-t_i) - \theta(t-t_j). \quad (31)$$

We have then performed numerical simulations of the system (1)–(3) for a device of 4 junctions with damping $\gamma=0.03$ and output resistance $R=10$, when the following parameters are used for the seed:

$$\lambda = 10^{-2}, \quad A_1 = 0.234, \quad A_2 = 0.402, \quad \Omega = 0.9, \quad (32)$$

and for the signal

$$\alpha_1 = 0.002, \quad \alpha_2 = 0.008,$$

$$t_1 = 2000, \quad t_2 = 3500, \quad t_3 = 5000, \quad t_4 = 9000. \quad (33)$$

The seed and signal are drawn on the left side of Fig. 6, the result of numerical simulations is displayed on the right side of Fig. 6. We conclude that the numerical simulation demonstrates the ability of the JJ parallel array to act as a digital amplifier with an efficiency (amplitude ratio) of about 50.

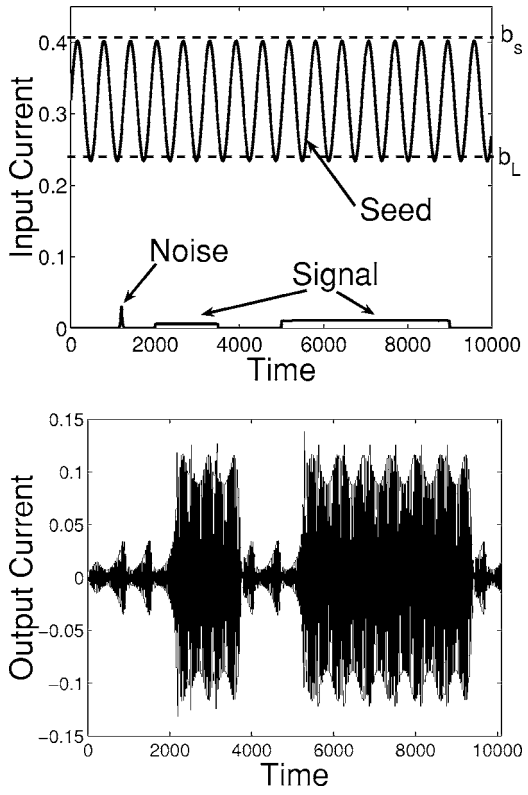

FIG. 6. Top: representation of the amplitude modulation of the rf-seed signal (29) and the corresponding finite time signals defined in (30). Bottom: Plot of the output current I_{out} that shows the net result of the signal amplification. Besides the two persistent signals, we also consider the pulselike fluctuation to show that the system is not sensitive to external small duration fluctuations or noise.

In order to check the influence of noise, or thermal fluctuations, we have included in the seed a small duration signal, as represented in Fig. 6. It appears that the system is very robust to such excitations, it reacts only on a persistent signal (with respect to the modulation time of the seed). The probability of getting a response to a pulselike fluctuation is negligible: it would require a fluctuation pulse located precisely at the time when the seed reaches its maximum value.

VII. CONCLUSION AND COMMENTS

The theory presented here demonstrates the possibility of realizing ultrasensitive detectors that can work in a large domain of frequencies (the whole forbidden bandgap of the Junction array), that need to be pumped with reasonable intensities (asymptotically vanishing near the band edge) and that produce a detection of any type of signal by macroscopic output (e.g., the rms intensity in the last junction). The realization of such a detector device would be worth it in the growing field of the q-bit detection problem, as described in Refs. 8 and 9. This detection ability can also be employed to conceive efficient digital amplifiers by a convenient modulation of the rf-seed.

By studying this question we have solved a problem that dates back to 1986,[1] namely the complete analytical understanding of the bistability in a long Josephson junction or in

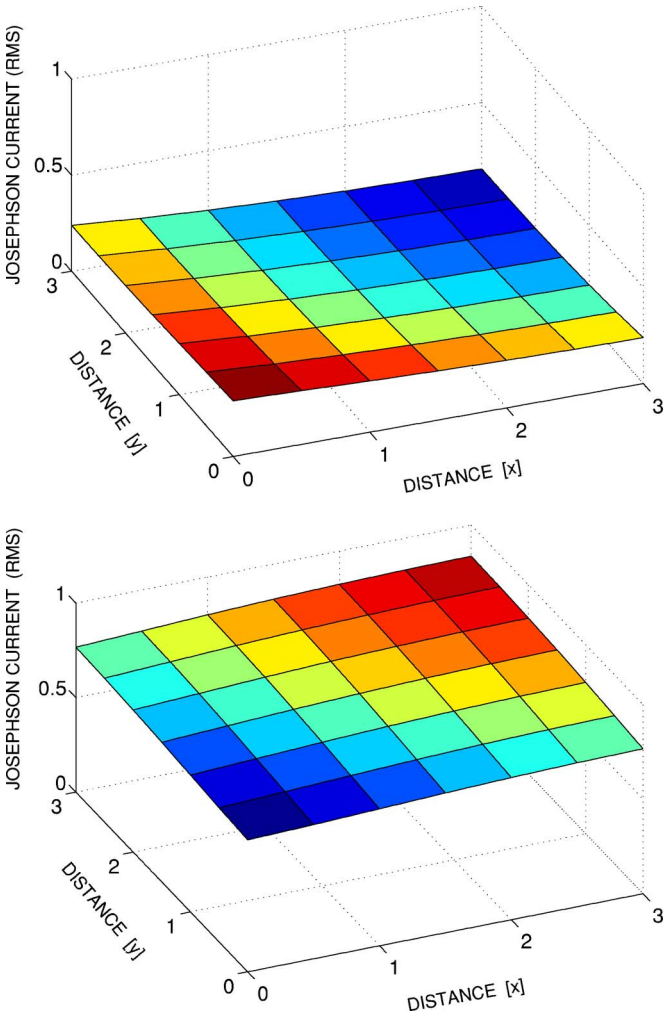

FIG. 7. (Color online) Bistable regime for the same driving parameters of a 2D Josephson lattice. The top graph represents the space distribution of rms values of the Josephson current in an unexcited regime. The bottom figure displays the excited stationary regime.

an array of short junctions. The practical usefulness of this result is the tool that allows us to compute the threshold seed amplitude where the device must be worked to become an ultrasensitive detector.

It should be noted here that our results apparently apply also to a long Josephson junction. However, in that case, the external driving (by an antenna) would influence the whole junction while for an array we can expect a device where only the first junction is excited (or at least only the first few junctions). Then we expect to be able to separate the output signal from the input in an array, which would be quite uneasy in a single long junction.

A straightforward generalization of the lattice model (2) to two dimensions allows us to simulate the bistable behavior, in the $N \times N$ Josephson junction array,

$$\ddot{u}_{m,n} + \gamma \dot{u}_{m,n} + \sin u_{m,n} - [u_{m,n+1} + u_{m,n-1} + u_{m+1,n} + u_{m-1,n} - 4u_{m,n}] = [\delta_{m1} + \delta_{n1}] f(t), \tag{34}$$

with free end boundary conditions $u_{m,1}=u_{m,0}$, $u_{m,N}=u_{m,N+1}$, $u_{1,n}=u_{m,0}$, $u_{N,n}=u_{N+1,n}$. The driving $f(t)$ is thus applied on the two boundaries $n=1$ and $m=1$ of the square lattice. As displayed in Fig. 7, we have obtained by numerical simulations that bistability is still present in this two dimensional (2D) system, which opens the interesting problem of the theoretical description of bistability in $2+1$ dimensions.

Another interesting issue is the generalization of this approach to the Josephson junction ladder,[19] where the model consists is a system of coupled sine-Gordon-like equations.[20]

ACKNOWLEDGMENTS

One of us (R. Kh.) thanks E. Goldobin for enlightening discussions regarding measurement techniques in Josephson junctions and acknowledges support by the Marie-Curie International Incoming Award (Contract No MIF1-CT-2005-021328) and NATO reintegration grant No. FEL.RIG. 980767.

[1] O. H. Olsen and M. R. Samuelsen, Phys. Rev. B **34**, 3510 (1986).
[2] D. Barday and M. Remoissenet, Phys. Rev. B **41**, 10387 (1990).
[3] H. S. J. van der Zant, M. Barahona, A. E. Duwel, T. P. Orlando, S. Watanabe, and S. Strogatz, Physica D **119**, 219 (1998).
[4] Y. S. Kivshar, O. H. Olsen, and M. R. Samuelsen, Phys. Lett. A **168**, 391 (1992).
[5] H. G. Winful, J. H. Marburger, and E. Garmire, Appl. Phys. Lett. **35**, 379 (1979).
[6] S. R. Shenoy and G. S. Agarwal, Phys. Rev. Lett. **44**, 1524 (1980).
[7] A. V. Ustinov, Physica D **123**, 315 (1998).
[8] I. Siddiqi, R. Vijay, F. Pierre, C. M. Wilson, L. Frunzio, M. Metcalfe, C. Rigetti, R. J. Schoelkopf, M. H. Devoret, D. Vion, and D. Esteve, Phys. Rev. Lett. **94**, 027005 (2005).
[9] I. Siddiqi, R. Vijay, F. Pierre, C. M. Wilson, M. Metcalfe, C. Rigetti, L. Frunzio, and M. H. Devoret, Phys. Rev. Lett. **93**, 207002 (2004).
[10] J. J. Chang, Phys. Rev. B **34**, 6137 (1986).
[11] M. Salerno, M. R. Samuelsen, G. Filatrella, S. Pagano, and R. D. Parmentier, Phys. Rev. B **41**, 6641 (1990).
[12] A. V. Ustinov, J. Mygind, and V. A. Oboznov, J. Appl. Phys. **72**, 1203 (1992); A. V. Ustinov, J. Mygind, N. F. Pedersen, and V. A. Oboznov, Phys. Rev. B **46**, 578 (1992).
[13] G. Costabile, R. D. Parmentier, B. Savo, D. W. McLaughlin, and A. C. Scott, Appl. Phys. Lett. **32**, 587 (1978).
[14] P. F. Byrd and M. D. Friedman, *Handbook of Elliptic Integrals For Engineers and Physicists* (Springer-Verlag, Berlin, 1954).
[15] R. Khomeriki and J. Leon, Phys. Rev. E **71**, 056620 (2005).
[16] Comparable results have been obtained in the case of Dirichlet boundary conditions to describe a pendula chain driven by a periodic torque whose frequency lies in the forbidden bandgap (Ref. 15). The Neuman boundary condition treated here, al-

though involving different solutions, leads to similar properties of bistability and supratransmission threshold.
[17] F. Geniet and J. Leon, Phys. Rev. Lett. **89**, 134102 (2002).
[18] F. Geniet and J. Leon, J. Phys.: Condens. Matter **15**, 2933 (2003).
[19] P. Binder, D. Abraimov, A. V. Ustinov, S. Flach, and Y. Zolotaryuk, Phys. Rev. Lett. **84**, 745 (2000); A. E. Miroshnichenko, M. Schuster, S. Flach, M. V. Fistul, and A. V. Ustinov, Phys. Rev. B **71**, 174306 (2005).
[20] E. Trias, J. J. Mazo, and T. P. Orlando, Phys. Rev. Lett. **84**, 741 (2000).